Aberration correction for time-domain ultrasound diffraction tomography

T. Douglas Mast[a)]
Applied Research Laboratory, The Pennsylvania State University, University Park, Pennsylvania 16802

(Received 9 August 2001; revised 26 March 2002; accepted 4 April 2002)

Extensions of a time-domain diffraction tomography method, which reconstructs spatially dependent sound speed variations from far-field time-domain acoustic scattering measurements, are presented and analyzed. The resulting reconstructions are quantitative images with applications including ultrasonic mammography, and can also be considered candidate solutions to the time-domain inverse scattering problem. Here, the linearized time-domain inverse scattering problem is shown to have no general solution for finite signal bandwidth. However, an approximate solution to the linearized problem is constructed using a simple delay-and-sum method analogous to ''gold standard'' ultrasonic beamforming. The form of this solution suggests that the full nonlinear inverse scattering problem can be approximated by applying appropriate angle- and space-dependent time shifts to the time-domain scattering data; this analogy leads to a general approach to aberration correction. Two related methods for aberration correction are presented: one in which delays are computed from estimates of the medium using an efficient straight-ray approximation, and one in which delays are applied directly to a time-dependent linearized reconstruction. Numerical results indicate that these correction methods achieve substantial quality improvements for imaging of large scatterers. The parametric range of applicability for the time-domain diffraction tomography method is increased by about a factor of 2 by aberration correction. [DOI: 10.1121/1.1481063]

PACS numbers: 43.20.Fn, 43.80.Qf, 43.60.Pt [LLT]

I. INTRODUCTION

This paper concerns time-domain diffraction tomography methods for solution of the time-domain inverse scattering problem, in which an unknown inhomogeneous medium is determined from its far-field acoustic scattering. This problem is of interest for medical ultrasonic imaging, since inverse scattering methods such as diffraction tomography can provide quantitative reconstruction of tissue properties including sound speed, density, and absorption.

Most practical inverse scattering methods to date have been based on linearization of the inverse problem using the Born or Rytov approximation.[1,2] These are weak scattering approximations, in which the variation of medium properties is assumed to be a small perturbation from a uniform background. Nonlinear inverse scattering methods,[3,4] which consider contributions of strong and multiple scattering, are much more complex and computationally intensive. However, since large-scale tissue structures cannot be considered weak scatterers at diagnostic ultrasound imaging frequencies,[5,6] linearized inverse scattering methods are of limited use for medical ultrasonic imaging.

A similar problem arises in conventional B-scan and synthetic-aperture imaging,[7,8] which form the basis for current diagnostic ultrasound scanners. Current scanners form synthetic images based on the assumption of a uniform background sound speed, which is essentially the Born approximation. The invalidity of this assumption is associated with image artifacts and focus aberration.[5,9] Considerable effort has been devoted to methods for aberration-corrected imaging, which is analogous to nonlinear inverse scattering. Approaches to aberration correction for pulse-echo imaging have been designed to correct distortion associated with several simplified propagation models, including refraction by homogeneous layers,[10,11] phase aberration close to the transducer aperture,[12–14] and aberration caused by a hypothetical phase screen away from the aperture.[15–17] All of these aberration correction methods require indirect estimation of the medium-induced distortion based on the received scattering data.

A time-domain diffraction tomography method has been introduced recently.[18,19] This method provides tomographic reconstructions of unknown scattering media from scattering data measured on a surface surrounding the region of interest, using the entire available bandwidth of the signals employed. The reconstruction algorithm is derived as a simple delay-and-sum formula similar to synthetic-aperture algorithms employed in conventional clinical scanners.[7,8] However, unlike current clinical scanners, the present method provides quantitative images of the spatially dependent tissue sound speed. These quantitative sound speed maps offer considerable potential for aberration correction, since the medium-induced distortion can be estimated directly from the image data.

The image reconstruction algorithm of Ref. 18 was derived from the frequency-domain exact solution to the linearized inverse scattering problem, i.e., diffraction tomography employing the Born approximation. Inverse scattering approaches based on the Born approximation form adequate

a)Current address: Ethicon Endo-Surgery, 4545 Creek Rd., ML 40, Cincinnati, OH 45242. Electronic mail: dmast@eesus.jnj.com

images only for relatively small, weakly scattering objects,[18,20] so that this approximation has limited utility for large-scale imaging problems such as ultrasonic mammography. In the present paper, an aberration correction approach, which significantly extends the range of validity of the time-domain diffraction tomography method, is introduced. The reconstruction method of Ref. 18 is shown to result in an approximate solution to the time-domain linearized inverse scattering problem; application of aberration correction results in reconstructions that better approximate the solution to the full nonlinear time-domain inverse problem.

Two related methods for aberration correction are presented here. The first, suggested by the synthetic-aperture nature of the reconstruction algorithm, employs a focus correction approach in which delays are computed from estimates of the medium using an efficient straight-ray approximation. The second approach is suggested by examination of the reconstruction itself in the time domain, as in Ref. 21. In this approach, delays are applied directly to a time-dependent linearized reconstruction. Numerical results show that both methods increase the parameter range for which valid images can be obtained and illustrate differences in performance between the two.

II. THEORY

The imaging problem considered here concerns reconstruction of an unknown medium from far-field, time-domain scattering measurements. Solutions of this inverse problem are quantitative images of scattering media such as biological tissue. Below, the linearized inverse scattering problem (e.g., quantitative ultrasonic imaging without aberration correction) is considered and shown to have no general solution. However, approximate solutions to the nonlinear inverse problem result in useful aberration correction methods for quantitative imaging.

A. The linearized time-domain inverse scattering problem

The time-domain inverse scattering problem analyzed below is defined as follows. A quiescent, inhomogeneous, fluid medium is subjected to an incident plane wave pulse propagating in the direction $\boldsymbol{\alpha}$,

$$p_i(\mathbf{r},t)=u(t-\mathbf{r}\cdot\boldsymbol{\alpha}/c_0), \tag{1}$$

where c_0 is a reference or ''background'' sound speed. The medium is assumed to have spatially varying sound speed, constant density, and no absorption, and to be completely characterized by a contrast function $\gamma(\mathbf{r})$, defined as

$$\gamma(\mathbf{r})=\frac{c_0^2}{c(\mathbf{r})^2}-1, \tag{2}$$

where $c(\mathbf{r})$ is the local sound speed at position $\mathbf{r}$. The inverse scattering problem is the determination of the medium contrast $\gamma(\mathbf{r})$ from time-domain measurements of the scattered field $p_s(\boldsymbol{\theta},\boldsymbol{\alpha},t)$ for all measurement directions $\boldsymbol{\theta}$, incident-wave directions $\boldsymbol{\alpha}$, and times t. The implicit neglect of density variations is not severely limiting, since the contrast given by Eq. (2) typically dominates reconstructed images even in the presence of density variations.[18]

A general time-domain solution for the scattered acoustic pressure at a far-field measurement radius R, valid for two-dimensional (2D) or three-dimensional (3D) scattering, is then

$$p_s(\boldsymbol{\theta},\boldsymbol{\alpha},t)=\mathbf{F}^{-1}[\hat{p}_s(\boldsymbol{\theta},\boldsymbol{\alpha},f)]\equiv\int_{-\infty}^{\infty}\hat{p}_s(\boldsymbol{\theta},\boldsymbol{\alpha},f)e^{-i2\pi ft}\,df, \tag{3}$$

where $\hat{p}_s(\boldsymbol{\theta},\boldsymbol{\alpha},f)$ is a single frequency component of the scattered wavefield, given in the far field by

$$\begin{aligned}\hat{p}_s(\boldsymbol{\theta},\boldsymbol{\alpha},f)&=\mathbf{F}[p_s(\boldsymbol{\theta},\boldsymbol{\alpha},t)]d\\&\equiv\int_{-\infty}^{\infty}p_s(\boldsymbol{\theta},\boldsymbol{\alpha},t)e^{i2\pi ft}\,dt\\&=k^2\Gamma(R,f)\int_{V_0}e^{-ik\boldsymbol{\theta}\cdot\mathbf{r}}\gamma(\mathbf{r}_0)\hat{p}_u(\mathbf{r},\alpha,\omega)\,dV_0.\end{aligned} \tag{4}$$

In Eq. (4), k is the wave number ω/c_0 and $\hat{p}_u(\mathbf{r}_0,\boldsymbol{\alpha},\omega)$ is the total frequency-domain acoustic pressure associated with an incident plane wave $\hat{u}(f)e^{ik\boldsymbol{\alpha}\cdot\mathbf{r}_0}$ [i.e., one frequency component of the plane wave pulse $u(t-\boldsymbol{\alpha}\cdot\mathbf{r}/c_0)$]. The integral in Eq. (4) is taken over the entire support of γ in $\mathbb{R}^2$ for 2D scattering or in $\mathbb{R}^3$ for 3D scattering. The term $\Gamma(R,f)$, associated with the far-field forms of the free-space Green's functions for the Helmholtz equation,[22] is

$$\begin{aligned}\Gamma(R,f)&=-\sqrt{\frac{i}{8\pi kR}}\quad\text{for } 2D \text{ scattering,}\\\Gamma(R,f)&=\frac{1}{4\pi r}\quad\text{for } 3D \text{ scattering.}\end{aligned} \tag{5}$$

The time-domain inverse scattering problem is given by the Fourier inverse of Eq. (4):

$$p_s(\boldsymbol{\theta},\boldsymbol{\alpha},t)=\int_V\mathbf{L}\left[p_u\left(\mathbf{r},\boldsymbol{\alpha},t-\frac{R}{c_0}+\frac{\boldsymbol{\theta}\cdot\mathbf{r}}{c_0}\right)\right]\gamma(\mathbf{r})\,dV, \tag{6}$$

where $p_u(\mathbf{r},\boldsymbol{\alpha},t)$ is the total time-domain acoustic pressure associated with the incident plane wave $u(t-\mathbf{r}\cdot\boldsymbol{\alpha}/c_0)$ and the linear operator $\mathbf{L}$ is defined as

$$\begin{aligned}&\mathbf{L}[p(\mathbf{r},\boldsymbol{\alpha},t)]\\&\quad=\frac{1}{c_0^2}\mathbf{F}^{-1}\left[\sqrt{\frac{i}{8\pi kR}}\mathbf{F}[\ddot{p}(\mathbf{r},\boldsymbol{\alpha},t)]\right]\quad\text{for } 2\text{D scattering,}\\&\mathbf{L}[p(\mathbf{r},\boldsymbol{\alpha},t)]=-\frac{1}{4\pi c_0^2R}\ddot{p}(\mathbf{r},\boldsymbol{\alpha},t)\quad\text{for } 3\text{D scattering.}\end{aligned} \tag{7}$$

Equation (6) defines a nonlinear inverse problem for the contrast $\gamma(\mathbf{r})$; the nonlinearity is associated with the dependence of $p(\mathbf{r},\boldsymbol{\alpha},t)$ on $\gamma(\mathbf{r})$.

The nonlinear time-domain inverse scattering problem defined by Eq. (6) can be linearized by invoking the Born approximation, in which the total acoustic pressure is approximated by the incident wave. The resulting linearized equation is

$$p_s(\boldsymbol{\theta},\boldsymbol{\alpha},t)=\int_V \mathbf{L}[u(t-\tau(\boldsymbol{\theta},\boldsymbol{\alpha},\mathbf{r}))]\,\gamma_L(\mathbf{r})\,dV, \tag{8}$$

where the true potential $\gamma(\mathbf{r})$ has been replaced by $\gamma_L(\mathbf{r})$, a hypothetical solution to the linearized inverse problem, and the propagation delay term $\tau(\boldsymbol{\theta},\boldsymbol{\alpha},\mathbf{r})$ is defined

$$\tau(\boldsymbol{\theta},\boldsymbol{\alpha},\mathbf{r})\equiv\frac{R}{c_0}-\frac{(\boldsymbol{\theta}-\boldsymbol{\alpha})\cdot\mathbf{r}}{c_0}. \tag{9}$$

The delay specified by Eq. (9) is precisely that required to refocus scattered waves through a homogeneous ($c=c_0$) medium onto each image point.

In the asymptotic weak scattering limit, the linearized inverse scattering problem (8) is equivalent to the original nonlinear problem (6), so that an exact solution for any waveform $u(t)$ is given by $\gamma_L(\mathbf{r})\rightarrow\gamma(\mathbf{r})$ as $\gamma(\mathbf{r})\rightarrow 0$. However, unlike the frequency-domain linearized inverse scattering problem, the inverse problem of Eq. (8) has no general solution for nonzero $\gamma(\mathbf{r})$. To prove this, one may examine the Fourier transform of Eq. (8), which is simply the linearization of Eq. (4):

$$\hat{p}_s(\boldsymbol{\theta},\boldsymbol{\alpha},f)=\Gamma(R,f)\hat{u}(f)\int_V e^{-ik(\boldsymbol{\theta}-\boldsymbol{\alpha})\cdot\mathbf{r}}\gamma_L(\mathbf{r})\,dV, \tag{10}$$

where k is the wave number $2\pi f/c_0$. Thus, any general time-independent solution of Eq. (8) must also be a frequency-independent solution to the linearized frequency-domain inverse scattering problem (10).

For $\boldsymbol{\theta}=\boldsymbol{\alpha}$ (the forward scattering case), Eq. (10) leads to the condition

$$\frac{\hat{p}_s(\boldsymbol{\theta},\boldsymbol{\theta},f)e^{-ikR}}{k^2\hat{u}(f)}=\frac{1}{4\pi R}\int_V \gamma_{\mathbf{L}}(\mathbf{r})dV=\text{const}\ (\forall f) \tag{11}$$

for existence of a general solution to Eq. (8). This requirement is easily seen by counterexample to be impossible. For example, Eq. (11) requires that, for all frequencies f, the magnitude of the forward scattered pressure should (for a unit-amplitude incident wave) be proportional to f^2. A counterexample is given by any high-contrast scatterer (e.g., $\gamma\sim 1$), for which this f^2 dependence occurs only at very low frequencies, such that the scatterer's dimensions are much smaller than the wavelength c_0/f.[23] Thus, although the nonlinear time-domain inverse scattering problem has an exact solution [equal to the true contrast $\gamma(\mathbf{r})$], the corresponding linearized problem has no general solution for arbitrary signal bandwidth except in the limiting case $\gamma\rightarrow 0$.

B. Approximate linearized solutions by Fourier synthesis

Although no solution $\gamma_L(\mathbf{r})$ to the quantitative imaging problem of Eq. (8) exists in general, one can still obtain approximate solutions by applying Fourier synthesis to the well-known exact solution of the frequency-domain linearized inverse scattering problem. For any frequency component of $p_s(\boldsymbol{\theta},\boldsymbol{\alpha},t)$, the frequency-domain linearized inverse problem (10) has an exact, frequency-dependent solution given by the frequency-domain filtered backpropagation formula.[2,24]

$$\gamma_B(\mathbf{r},f)=\frac{\hat{\mu}(f)e^{-ikR}}{\hat{u}(f)}\int\int \Phi(\boldsymbol{\theta},\boldsymbol{\alpha})\hat{p}_s(\boldsymbol{\theta},\boldsymbol{\alpha},f)\times e^{ik(\boldsymbol{\theta}-\boldsymbol{\alpha})\cdot\mathbf{r}}\,dS_\alpha\,dS_\theta, \tag{12}$$

where

$$\hat{\mu}(f)=\sqrt{\frac{kR}{8i\pi^3}},\quad \Phi(\boldsymbol{\theta},\boldsymbol{\alpha})=|\sin(\theta-\alpha)|\ \text{ in 2D},$$
$$\hat{\mu}(f)=\frac{kR}{4\pi^3},\quad \Phi(\boldsymbol{\theta},\boldsymbol{\alpha})=|\boldsymbol{\theta}-\boldsymbol{\alpha}|\ \text{ in 3D}. \tag{13}$$

Each surface integral in Eq. (12) is performed over the entire measurement circle for the 2D case and over the entire measurement sphere for the 3D case.

Fourier inversion of Eq. (10) into the time domain can be performed using the convolution theorem.[25] The result, with the hypothetical linearized solution $\gamma_L(\mathbf{r})$ replaced by the Born reconstruction $\hat{\gamma}_B(\mathbf{r},f)$, is

$$p_s(\boldsymbol{\theta},\boldsymbol{\alpha},t)=-\frac{1}{4\pi c_0^2 R}\int_V \ddot{u}(t-\tau(\boldsymbol{\theta},\boldsymbol{\alpha},\mathbf{r}))\otimes\gamma_B(\mathbf{r},t)\,dV, \tag{14}$$

where $\gamma_B(\mathbf{r},t)$ is the inverse Fourier transform of the frequency-domain solution $\hat{\gamma}_B(\mathbf{r},f)$. The time-domain reconstruction $\gamma_B(\mathbf{r},t)$ is an exact solution of the integral equation (14), which is similar but not equivalent to the linearized time-domain inverse scattering problem of Eq. (8). Because $\hat{\gamma}_B(\mathbf{r},f)$ is conjugate symmetric, the time-domain potential $\gamma_B(\mathbf{r},t)$ is purely real.[21]

Comparison of Eqs. (8) and (14) shows that, in the weak scattering limit,

$$\gamma_B(\mathbf{r},t)\rightarrow\gamma(\mathbf{r})\,\delta(t)+\psi(\mathbf{r},t), \tag{15}$$

where $\psi(\mathbf{r},t)$ is a "nonradiating source"[26] that satisfies the constraint

$$\int_V \ddot{u}(t-\tau(\boldsymbol{\theta},\boldsymbol{\alpha},\mathbf{r}))\otimes\psi(\mathbf{r},t)\,dV=0. \tag{16}$$

The presence of the nonradiating source term $\psi(\mathbf{r},t)$ is consistent with the nonuniqueness of solutions to Eq. (14).[27] For example, additional solutions to Eq. (14) include the class of functions $\gamma_B(\mathbf{r},t)+\phi(\mathbf{r})$, where $\phi(\mathbf{r})$ is the inverse Fourier transform of any function $\hat{\phi}(\mathbf{k})$ that is zero inside the Ewald sphere,[1] defined for the upper frequency limit of the incident pulse as $\mathbf{k}\leqslant 4\pi f_h/c_0$, where f_h is the upper limit of the pulse frequency content.

A straightforward approach to estimate $\gamma_B(\mathbf{r},t)$ [and thus $\gamma(\mathbf{r})$] is to perform inverse Fourier transformation on the frequency-domain Born inversion $\hat{\gamma}_B(\mathbf{r},f)$. A natural estimate of the medium contrast is a reconstruction employing information from multiple frequencies contained in the incident pulse, e.g.,

$$\gamma_v(\mathbf{r},t)=\int_{-\infty}^{\infty}\hat{\gamma}_B(\mathbf{r},f)\hat{v}(f)e^{-2\pi ift}\,df\Big/\int_{-\infty}^{\infty}\hat{v}(f)\,df \tag{17}$$

$$=\gamma_B(\mathbf{r},t)\otimes v(t)/v(0) \tag{18}$$

$$\approx\gamma(\mathbf{r})v(t)/v(0), \tag{19}$$

where the final expression results from Eq. (15). The frequency weight $\hat{v}(f)$ must be integrable and have no support outside the support of $\hat{u}(f)$, but is otherwise arbitrary. The time dependence of the reconstructed contrast can be removed from Eq. (19) by setting $t=0$ (called the "imaging condition" in Ref. 28).

If the incident waveform is sinusoidal, so that, for instance, $\hat{u}(f)=\delta(f-f_0)+\delta(f+f_0)$, the reconstructed potential $\gamma_v(\mathbf{r},0)$ is equal to the real part of the frequency-domain solution $\hat{\gamma}_B(\mathbf{r},f_0)$. Thus, $\gamma_v(\mathbf{r},0)$ is an exact solution of the linearized inverse problem in the single-frequency limit. However, as proven above, no time-independent reconstruction can solve the general linearized time-domain inverse scattering problem, so that $\gamma_v(\mathbf{r},0)$ is only an *approximate* solution for any nonzero-bandwidth incident waveform $u(t)$.

The Fourier inversion of Eq. (17) can be performed either numerically or analytically. Numerical inversion, using frequency-domain reconstructions at a number of discrete frequencies within the bandwidth of the incident pulse, was the approach employed by Lin, Nachman, and Waag.[21] (However, the frequency-domain inversions of Ref. 21 were performed using eigenfunctions of the far-field scattering operator[29] instead of filtered backpropagation.) Alternatively, particular choices of the weight $\hat{v}(f)$ allow analytic inversion of the frequency-domain reconstruction $\gamma_B(\mathbf{r},f)$ into the time domain, resulting in a simple delay-and-sum formula. For the weight $\hat{v}(f)=\hat{u}(f)/\hat{\mu}(f)H(f)$, where $H(f)$ is the Heaviside step function, the resulting formula is

$$\gamma_v(\mathbf{r},t)=\mathrm{Re}\left[\frac{1}{N}\int\int\Phi(\boldsymbol{\theta},\boldsymbol{\alpha})(p_s(\boldsymbol{\theta},\boldsymbol{\alpha},\tau)+i\mathbf{H}^{-1}[p_s(\boldsymbol{\theta},\boldsymbol{\alpha},\tau)])\,dS_\alpha\,dS_\theta\right], \tag{20}$$

where

$$N=2\int_0^{\infty}\frac{\hat{\mu}(f)}{\hat{\mu}(f)}df, \tag{21}$$

τ is given by Eq. (9), and $\mathbf{H}^{-1}$ is the inverse Hilbert transform operator (quadrature filter), which results from limiting frequency integration to the interval $(0,\infty)$.[18]

The reconstruction formula of Eq. (20) is identical to that derived in Ref. 18 and similar to that derived in Ref. 30. In view of the present derivation, these previous methods are understood to provide approximate solutions to the linearized time-domain inverse scattering problem (8).

C. Aberration-corrected solutions

The form of the approximate linearized solution derived above suggests possible approaches to improvement of images beyond the limits of the Born approximation.

First, one may observe that the reconstruction formula of Eq. (20) synthetically focuses the time-domain scattered field back onto each point in the medium.[18] This observation leads to the idea of aberration correction by iterative refinement of the focus quality. Since the reconstruction provides an estimate of the medium itself, this refinement is fairly straightforward. One simple implementation employs an assumption that background inhomogeneities result only in cumulative delays (or advances) of the incident and scattered wavefronts, so that the total delay for an angle ϕ and a point position $\mathbf{r}$ is given by

$$\delta\tau(\boldsymbol{\phi},\mathbf{r})=\int_{\xi}c(\boldsymbol{\xi})^{-1}d\xi-\frac{R}{c_0}, \tag{22}$$

where the integral is performed along the line that joins the spatial points $\mathbf{r}$ and $R\boldsymbol{\phi}$, Aberration-corrected reconstructions can then be performed using Eq. (20) with τ replaced by the corrected delay term

$$\tau\rightarrow R/c_0+\frac{(\boldsymbol{\alpha}-\boldsymbol{\theta})\cdot\mathbf{r}}{c_0}+\delta r(\boldsymbol{\alpha},\mathbf{r})+\delta\tau(\boldsymbol{\theta},\mathbf{r}) \tag{23}$$

and by then computing $\gamma_v(\mathbf{r},0)$ using Eq. (20).

An alternative approach to aberration correction is motivated by the observation, made in Ref. 21, that temporal delays from wave propagation in the inhomogeneous medium result in corresponding delays to the time-domain reconstruction of Eq. (17). That is, the reconstructed waveforms $\gamma_v(\mathbf{r},t)$ may be delayed or advanced relative to the waveform $v(t)$. In Ref. 21, correction for this temporal aberration was implemented by adaptive demodulation of $\gamma_v(\mathbf{r},t)$ from the weighting waveform $v(t)$. Here, envelope detection is applied to $\gamma_v(\mathbf{r},t)$ and the time of maximum envelope amplitude $t_{\max}$ is found for each point $\mathbf{r}$, resulting in the aberration-corrected reconstruction

$$\gamma(\mathbf{r})\approx\gamma_v(\mathbf{r},t_{\max}(\mathbf{r})). \tag{24}$$

Envelope detection can also be applied to iterative reconstructions obtained using the focus correction given by Eq. (22).

III. COMPUTATIONAL METHODS

The present aberration correction methods have been tested using simulated scattering data for a number of two-dimensional test objects. The computational configuration was chosen to mimic the characteristics of an available 2048-element ring transducer.[31] The time-domain waveform employed for all the computations reported here was

$$u(t)=\cos(\omega_0 t)e^{-t^2/(2\sigma^2)}, \tag{25}$$

where $\omega_0=2\pi f_0$ for a center frequency of f_0, taken here to be 2.5 MHz, and σ is the temporal Gaussian parameter. The value of σ chosen here was 0.25, which corresponds to a -6-dB bandwidth of 1.5 MHz.

For 2D cylindrical inhomogeneities, the frequency-domain scattered field $\hat{p}_s(\boldsymbol{\theta},\boldsymbol{\alpha},\omega)$ was computed using an exact series solution[32] for each frequency component of interest. In implementation of the series solution, summations were truncated when the magnitude of a single coefficient

dropped below 10^{-12} times the sum of all coefficients. These single-frequency solutions, which correspond to Fourier coefficients of the time-domain scattered field, were weighted and inverted by discrete Fourier transform to obtain the exact time-domain scattered field associated with the incident pulse of Eq. (25). Scattering from cylinders of radius 4.0 mm and contrasts ranging from $\gamma=0.001$ to $\gamma=0.14$ was computed on a measurement circle of radius 176 mm for 384 incident-wave directions and 96 measurement directions. The sampling rate employed was 9.14 MHz.

Solutions were also obtained for a large-scale breast model using a time-domain *k*-space method.[33] The breast model was obtained by image processing a coronal cross section of three-dimensional photographic data from the Visible Human Female data set with a pixel size of 0.333 mm. Hue, saturation, and value were mapped to sound speed and density using empirically determined relations. Sound speed and density were assumed to be linearly proportional; this assumption is realistic for mammalian soft tissues.[34,35]

Sound speed and density maps were smoothed using a Gaussian filter to reduce artifacts associated with the slicing process. (The tissue map employed is shown in Fig. 3.) This tissue model was scaled down by a factor of 0.6 from the original data set and mapped onto a grid of 512×512 points with a spatial step of 0.111 mm. A time step of 0.0546 μs, corresponding to a Courant–Friedrichs–Lewy number of 0.75, was employed. Based on the scaling of the tissue model, the scattered field obtained is equivalent to that of the full-scale breast model (largest dimension 75 mm) for a center frequency of 0.5 MHz.

Scattered acoustic pressure signals were recorded at a sampling rate of 9.15 MHz for 128 incident-wave directions. A circle of 512 simulated point receivers, which had a radius of 9.0 mm in these computations (equivalent to a radius of 45 mm for a 0.5 MHz center frequency), completely contained the scaled-down breast model. Far-field waveforms were computed by Fourier transforming the time-domain waveforms on the near-field measurement circle, transforming these to far-field waveforms for each frequency using a numerically exact transformation method,[21,36] and performing inverse Fourier transformation to yield time-domain far-field waveforms at a measurement circle of radius 234 cm (or 1170 mm if scaled to a 0.5 MHz center frequency). All forward and inverse temporal Fourier transforms, as well as angular transforms occurring in the near-field–far-field transformation, were performed by fast Fourier transforms (FFTs).[37]

The time-domain imaging method was directly implemented using Eq. (20), evaluated using straightforward numerical integration over all incident-wave and measurement directions employed. In one implementation, similar to that from Ref. 18, images were evaluated only for the time $t=0$. In this case, before evaluation of the argument τ for each signal, the time-domain waveforms were resampled at a sampling rate of 16 times the original rate. This resampling was performed using FFT-based Fourier interpolation. The inverse Hilbert transform was implicitly performed using the same FFT operation. Values of the pressure signals at the time τ were then determined using linear interpolation between samples of the oversampled waveforms. The integrals of Eq. (20) were implemented using discrete summation over all transmission and measurement directions employed.

In the implementation of reconstructions for multiple times, storage and computation time requirements necessitated modification of the algorithm implementation. For multiple-time reconstructions, a reconstruction of $\gamma_v(\mathbf{r},t)$ at the sampling rate of the scattering data was first obtained by direct integration. Delays of the time-domain scattered waveforms were implemented using cubic spline interpolation.[38] Reconstructions were performed for an interval of length 2.4 μs, multiplied by a window with cosine tapers of length 0.6 μs at each end, and upsampled by a factor of 8 using Fourier interpolation. Inverse Hilbert transformation of $\gamma_v(\mathbf{r},t)$ was performed by the same FFT operation used to implement the Fourier interpolation. Finally, the temporal position of the envelope peak was found from the zero crossing of the envelope derivative,

$$\frac{\partial\left|\gamma_v(\mathbf{r},t_{\text{peak}})+iH^{-1}[\gamma_v(\mathbf{r},t_{\text{peak}})]\right|}{\partial t}=0. \tag{26}$$

The derivative in Eq. (26) was evaluated using a second-order-accurate center-difference scheme.

Focus correction was implemented using a straight-ray approximation, which is based on the assumption that background inhomogeneities result only in cumulative delays (or advances) of the incident and scattered wavefronts. In this approximation, the total delay for an image position $\mathbf{r}$ and a direction $\boldsymbol{\phi}$ is given by Eq. (22) and aberration-corrected reconstructions are performed using Eq. (20) with τ replaced by the corrected delay term of Eq. (23). The path integrals of Eq. (23) were performed using an algorithm based on the digital differential analyzer (DDA) image processing method.[39] This method very efficiently finds the nearest neighbors to a line of specified starting position and slope; thus, the integrals can be evaluated by simple summation without any need for interpolation. To account for variable step size along the integration path, this summation is normalized by multiplication with L/N, where L is the length of the specified line and N is the number of points employed in the summation. Since the reconstruction process acts in part as a low-pass filter, the integral performed using nearest neighbors to the line of interest is sufficiently accurate.

Iterative focus correction was performed by first constructing an uncorrected image, either for $t=0$ or $t=t_{\text{peak}}$. The reconstructed sound speed was then employed to evaluate the delay corrections of Eq. (23) using the DDA implementation of the integrals from Eq. (22). To avoid spurious modification of image points outside the support of the scatterer, the delay term of Eq. (23) was multiplied by the factor

$$A=\begin{cases}1, & |\gamma_v(\mathbf{r})|\geq\gamma_{\max}/2,\\ (1-\cos[2\pi|\gamma_v(\mathbf{r})|/\gamma_{\max}])/2, & |\gamma_v(\mathbf{r})|<\gamma_{\max}/2,\end{cases} \tag{27}$$

where $\gamma_{\max}$ is the maximum value of $|\gamma_v(\mathbf{r})|$ for the previous reconstruction and the temporal criterion ($t=0$ or $t=t_{\text{peak}}$) employed.

Iteration proceeded as follows. A new reconstruction was compared to the previous reconstruction; if the relative

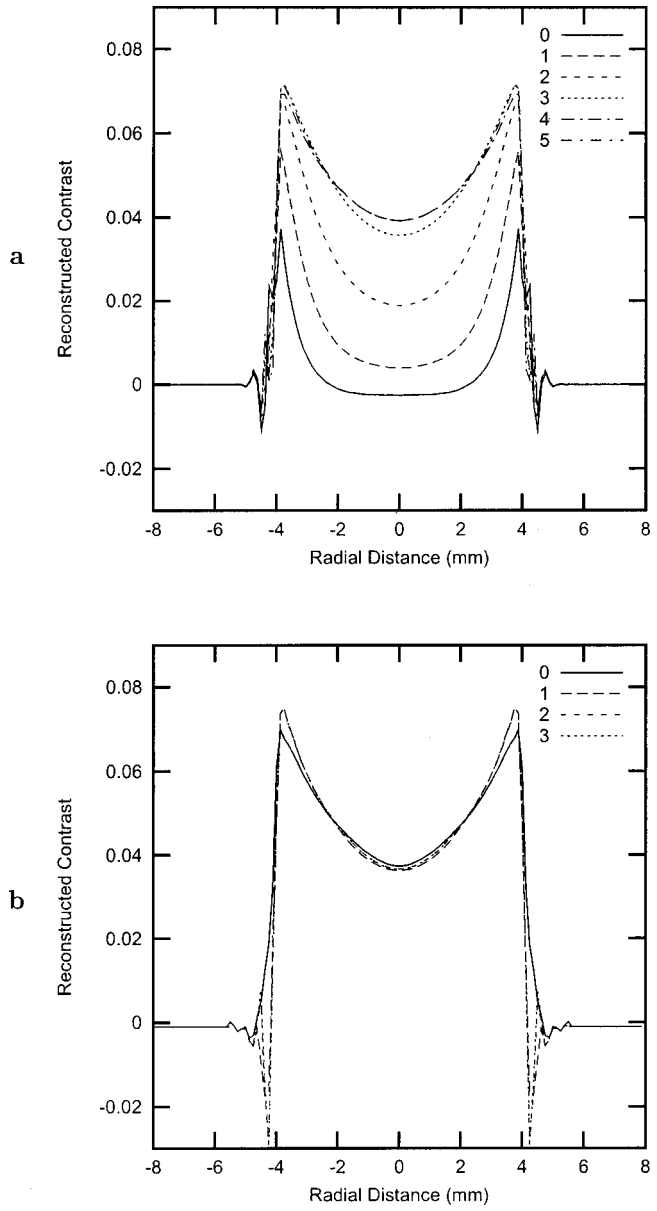

FIG. 1. Cross sections of time-domain reconstructions with adaptive focus correction for both imaging criteria. Reconstructions are of a homogeneous cylinder with a radius of 4 mm ($ka=41.2$) and a contrast $\gamma=0.08$. In each case, the "0" curve refers to an uncorrected reconstruction, while curves labeled "1" and higher correspond to subsequent iterations of focus correction. (a) $t=0$. (b) $t=t_{\text{peak}}$.

rms error between the two was greater than 5%, further iterations were carried out up to a prescribed maximum number of iterations, taken here to be 20. The criterion of 5% was chosen because image quality was not substantially enhanced by use of lower error thresholds. Due to the efficiency of the delay computation, each iteration required about the same computation time as the original reconstruction.

IV. NUMERICAL RESULTS

The performance of aberration-corrected time-domain diffraction tomography imaging, using the two approaches introduced above, is illustrated by the numerical examples presented in this section.

Figure 1 shows reconstructions of a homogeneous cylinder with a radius of 4 mm and a contrast $\gamma=0.08$. For the center frequency of 2.5 MHz, this corresponds to a nondimensional radius $ka=41.2$. Panel (a) shows cross sections of reconstructions obtained using the $t=0$ criterion. The "0" curve refers to an uncorrected (Born approximation) reconstruction, while curves labeled "1" and higher correspond to subsequent iterations of focus correction performed using the delay correction of Eq. (23) as described in Sec. III. Panel (b) shows corresponding cross sections obtained using the $t=t_{\text{peak}}$ criterion. One may observe that iterative focus correction greatly improves reconstructions for the $t=0$ criterion. The initial (Born) reconstruction shows mainly the edges of the cylinder; further iterations improve the accuracy within the cylinder interior. This process somewhat resembles the inverse scattering method of layer stripping,[40,41] in which an unknown medium is iteratively reconstructed with each iteration probing further into the medium interior.

In contrast, iterative focus correction provides little, if any, improvement to the reconstructions obtained using the $t=t_{\text{peak}}$ criterion [Fig. 1(b)]. In this case, the initial reconstruction captures the cylinder interior very well. Further iterations slightly increase the reconstructed contrast near the edges, but also introduce artifacts not present in the initial reconstruction. After convergence, the reconstructed value is more accurate than the $t=0$ image for the cylinder edges but less accurate for the interior.

For the reconstructions shown in Fig. 1, images of size 128×128 pixels were computed from time-domain scattering data for 96 incident-wave directions and 384 measurement directions. The computation time required on a 650-Mhz Athlon processor was about 6 CPU min per iteration for the $t=0$ image criterion (about 38 min total for the six iterations performed) and about 45 CPU min per iteration for the $t=t_{\text{peak}}$ criterion.

The relative performance of iterative focus correction using the two image criteria is illustrated in Fig. 2. Here, reconstructions were based on exact scattering data for a 4-mm cylinder with contrast $0.01\leqslant\gamma\leqslant0.12$. Since previous studies have shown that the accuracy of diffraction tomography reconstructions is roughly a function of the nondimensional parameter $ka\cdot\gamma$,[18,20] the relative error is plotted as a function of this nondimensional parameter. The Born approximation is considered to provide useful images for cylinders up to $ka\cdot\gamma\sim2$;[18,20] by this standard, the iterative focus correction implemented here increases the upper limit of validity for $t=0$ images to $ka\cdot\gamma\sim4$. As in Fig. 1, iterative focus correction is seen to provide little improvement in accuracy for images obtained using the $t=t_{\text{peak}}$ criterion. The quantitative accuracy of reconstructions is slightly increased by iteration for large values of the parameter $ka\cdot\gamma$, but can be slightly diminished for smaller values. Also notable is that iteration using the $t=0$ criterion fails completely above $ka\cdot\gamma\sim4$, while the $t=t_{\text{peak}}$ criterion reaches a comparable error level around $ka\cdot\gamma\sim4$ and then increases gradually in error with increasing scatterer contrast.

Quantitative images of a large-scale 2D breast model, used to generate simulated scattering data in the manner described in Sec. IV, are shown in Figs. 3 and 4. Panel (a) of Fig. 3 shows the 2D model used to generate the synthetic

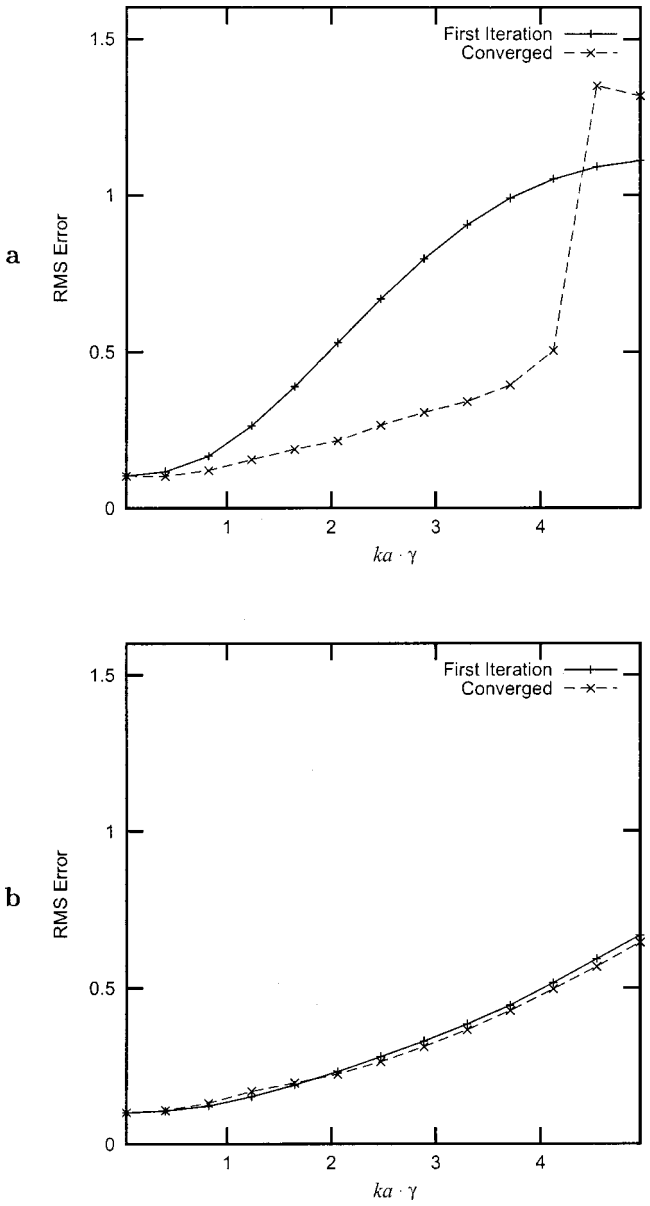

FIG. 2. The rms error for reconstructions of a 4.0-mm-radius cylinder with both imaging criteria, with adaptive focus correction (solid lines) and without (dashed lines). (a) $t=0$. (b) $t=t_{\text{peak}}$.

data. For this model, the parameter $ka \cdot \gamma$ is about 9.3 if estimated using the sound speed of fat, the center frequency of 0.5 MHz, and the largest half-dimension of 37.5 mm. However, a more conservative estimate employing the average contrast γ within the scatterer yields $ka \cdot \gamma \sim 2.8$, which meets the accuracy criterion $ka \cdot \gamma < 4$ determined from the cylinder simulations. Panel (b) of Fig. 3 shows the image reconstructed using the $t=t_{\text{peak}}$ criterion without any focus correction. In this case, the reconstructed image appears to be artifactually sharpened compared to the original model. Although there is a close correspondence between most features of the model and the reconstruction, some differences exist. For example, the reconstructed skin thickness is significantly smaller than that of the actual model in several locations.

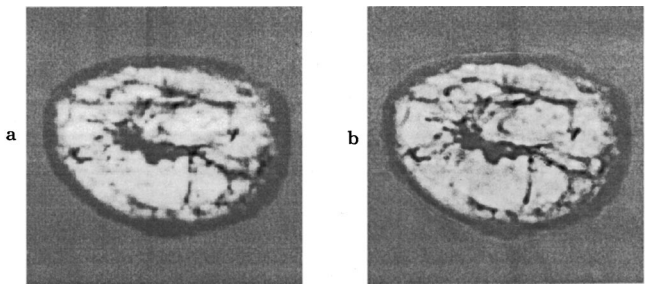

FIG. 3. Reconstruction of a large-scale two-dimensional breast model from simulated scattering data. (a) Model. (b) Initial time-domain reconstruction using $t=t_{\text{peak}}$ criterion.

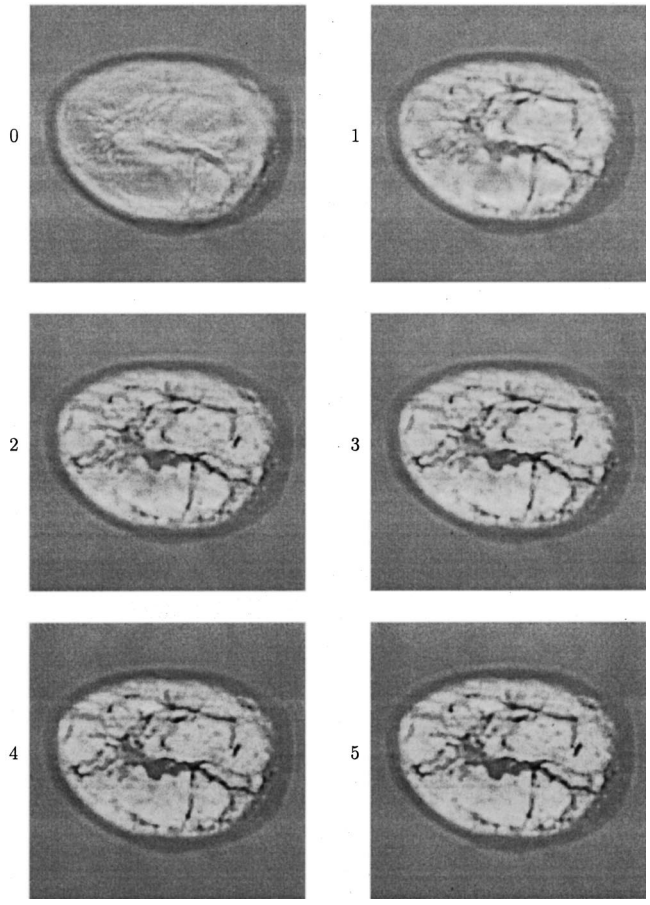

FIG. 4. Images of the large-scale breast model obtained using the $t=0$ criterion with adaptive focusing. Panel 0 shows the initial (linear) reconstruction and panels 1–5 show the subsequent iterations up to convergence.

Reconstructions of the 2D breast model, obtained using the $t=0$ criterion and iterative focus correction, are shown in Fig. 4. In this case, the initial (Born) reconstruction renders the skin layer fairly well, but the interior of the breast model is reconstructed poorly. Subsequent iterations improve the rendering of the connective and glandular tissue structure within the breast. Both focus quality and quantitative accuracy of the reconstructions improve with iteration. The converged reconstruction (iteration 5) resembles a low-pass filtered version of the original model [Fig. 3(a)] except for a small area of spuriously high reconstructed contrast within the interior glandular tissue.

Both reconstruction criteria successfully image the sound speed variation of the 2D breast model, even though the model also included realistic density variations. This re-

sult is expected, since diffraction tomography images of sound speed are not greatly degraded by any density variations that are small and fairly smooth.[18] These criteria are met by the breast model employed here, in which the density variations were of comparable magnitude to the small (maximum about 6%) sound speed variations.

For the large-scale 2D breast model, computation times required for 256×256 pixel images, 128 incident-wave directions, and 512 measurement directions were about 1.3 CPU h per iteration for the $t=0$ image criterion (8.0 h for the six iterations up to convergence) and about 4.6 CPU h for the initial reconstruction using the $t=t_{\text{peak}}$ criterion.

V. DISCUSSION

The two abberation correction methods considered here may be compared as follows. Both methods have the effect of improving the alignment of the time-domain reconstruction $\gamma_v(\mathbf{r},t)$. In the case of $t=0$ images with adaptive focus correction, the time-domain reconstruction is implicitly aligned by compensation for propagation delay within the inhomogeneous medium. The $t=t_{\text{peak}}$ criterion can be thought of as an explicit alignment of the time-domain reconstruction.

Previous qualitative studies of the validity of the Born approximation[18,20] have established a threshold for valid Born reconstructions at $ka\cdot\gamma\sim2$, which corresponds to a normalized rms error of about 0.5 (Fig. 2). Given this somewhat arbitrary threshold for the maximum allowable error, both aberration correction methods employed here have a similar range of validity, up to about $ka\cdot\gamma\sim4$. Thus, either approach extends the parametric range of validity for time-domain diffraction tomography by about a factor of 2.

Each image criterion also introduces characteristic artifacts. The $t=0$ criterion with adaptive focusing acts in part as a low-pass filter to reconstructions, consistent with the well-known low-pass filtering effect of conventional diffraction tomography.[1] The $t=t_{\text{peak}}$ criterion introduces edge artifacts that have the qualitative effect of artifactually sharpening images. More robust methods of delay estimation, such as cross-correlation between the time-domain reconstruction $\gamma_v(\mathbf{r},t)$ and the modulating waveform $v(t)$,[21] may provide better reconstruction quality than the $t=t_{\text{peak}}$ criterion, particularly for scattering data corrupted by noise or measurement imprecision.

The $t=0$ image criterion can provide faster reconstructions, since the reconstructed contrast $\gamma_v(\mathbf{r},t)$ needs only to be evaluated for one time. However, for large or high-contrast scatterers, iterative aberration correction is necessary to obtain high-quality reconstructions. The $t=t_{\text{peak}}$ criterion requires longer computation time for each reconstruction; however, because this criterion implicitly incorporates a form of aberration correction, subsequent iterations provide little additional benefit. As a result, computation times required for a given level of accuracy can be comparable for either image criterion.

Notable is that reconstruction quality, as characterized by criteria such as the point-spread function of a quantitative image, can be improved by optimization of the weight $\hat{v}(f)$.[21] Although the delay-and-sum reconstruction formula (20) depends on a frequency weight determined by the incident waveform $u(t)$, any desired weight $\hat{v}(f)$ can still be applied by preprocessing of the scattering data. That is, the inverse problem associated with an arbitrary incident waveform $w(t)$ (such as the impulse response of a particular electroacoustic transducer) can be transformed into the inverse problem associated with a desired waveform $u(t)$ by applying the deconvolution operation

$$[p_s(\boldsymbol{\theta},\boldsymbol{\alpha},t)]_{u(t)}=\mathbf{F}^{-1}\left[\frac{\hat{u}(f)}{\hat{w}(f)}\mathbf{F}[p_s(\boldsymbol{\theta},\boldsymbol{\alpha},t)]_{w(t)}\right], \tag{28}$$

where $\mathbf{F}$ denotes temporal Fourier transformation, to the measured scattering data. This operation transforms the measured data into the corresponding data that would be measured using an optimal incident pulse $u(t)$. For reasons of stability, the effective bandwidth of $\hat{u}(f)$ should be comparable to that of $\hat{w}(f)$ (as determined, for instance, by the noise floor of a given measurement).

The adaptive focusing implemented here employed a simple straight-ray approximation for wavefront aberration incurred in tissue. However, the principle of aberration correction by adaptive focusing should allow greater improvements to be gained using more complete distortion models. For example, the distortion caused by a strongly scattering medium can be accurately modeled using a full-wave computational method such as that of Ref. 33. In principle, appropriate deconvolution could be employed to remove the effects of the intervening medium for each incident-wave direction, measurement direction, and image location, so that an aberration-corrected reconstruction could then be performed by applying Eq. (20) to the corrected scattering data. In some cases, *a priori* information on the scattering medium may be exploited to improve the convergence of such adaptive focusing algorithms. This basic approach, in which a linearized reconstruction is performed on scattering data that has been transformed to remove higher-order scattering effects, is common to a number of existing nonlinear inverse scattering methods.[42]

The methods of aberration correction proposed here differ from most adaptive imaging methods for pulse-echo ultrasound (e.g., Refs. 12 and 16) because adaptive focusing is performed using a direct reconstruction of the medium rather than a simpler distortion estimate. Thus, aberration correction using quantitative imaging methods could be of great interest for pulse-echo systems such as current clinical scanners. However, the limited spatial-frequency information provided in pulse-echo mode[1,18] reduces the quality of quantitative images of this kind. One possible approach to increasing the spatial-frequency content of pulse-echo quantitative images could be to apply deconvolution to the scattered signals.[43–45] If such deconvolution methods could increase the spatial-frequency coverage sufficiently to obtain accurate (although possibly low-resolution) quantitative sound-speed maps, such maps could be employed directly for adaptive focusing in pulse-echo images.

VI. CONCLUSIONS

Two related approaches to aberration correction for quantitative ultrasonic imaging have been presented. These methods are based on approximate solutions to the linearized time-domain inverse scattering problem, implemented using adaptations of two previous time-domain diffraction tomography methods.[18,21] One approach, based on a delay-and-sum reconstruction formula, applies adaptive focusing based on estimates of the scattering medium. The other approach implements aberration correction by applying appropriate delays to a time-dependent reconstruction.

Numerical results show that each of the considered aberration correction approaches increases the parametric range of validity for time-domain diffraction tomography by about a factor of 2. The extended range of validity is sufficient to allow effective quantitative imaging of large-scale scattering media, such as the 75-mm breast model imaged here at 0.5 MHz. Adaptive focusing correction based on more complete scattering models could further increase this range of validity. Given sufficient *a priori* information on the unknown medium, the principle of focus correction may allow accurate quantitative images to be obtained for strongly-scattering media at larger scales and higher frequencies.

The approaches presented here may also be useful for aberration correction in pulse-echo imaging. If sufficiently broadband information can be extracted from pulse-echo scattering data, the time-domain diffraction tomography methods considered here may allow quantitative tissue characterization using clinically convenient measurement configurations. Quantitative maps obtained in this manner would also be useful as medium models for aberration correction in conventional B-scan and synthetic-aperture imaging.

ACKNOWLEDGMENTS

This work was supported by the Breast Cancer Research Program of the U.S. Army Medical Research and Materiel Command under Grant No. DAMD17-98-1-8141. Any opinions, findings, conclusions, or recommendations expressed in this publication are those of the author and do not necessarily reflect the views of the U.S. Army. The author is grateful for helpful discussions with James F. Kelly, Adrian I. Nachman, Feng Lin, and Robert C. Waag.

[1] E. Wolf, ''Three-dimensional structure determination of semi-transparent objects from holographic data,'' Opt. Commun. **1**, 153–156 (1969).
[2] A. J. Devaney, ''Inversion formula for inverse scattering within the Born approximation,'' Opt. Lett. **1**, 111–112 (1982).
[3] D. T. Borup, S. A. Johnson, W. W. Kim, and M. J. Berggren, ''Nonperturbative diffraction tomography via Gauss-Newton iteration applied to the scattering integral equation,'' Ultrason. Imaging **14**, 69–85 (1992).
[4] S. Gutman and M. Klibanov, ''Two versions of quasi-Newton method for multidimensional inverse scattering problem,'' J. Comput. Acoust. **1**, 197–228 (1993).
[5] L. M. Hinkelman, D.-L. Liu, R. C. Waag, Q. Zhu, and B. D. Steinberg, ''Measurement and correction of ultrasonic pulse distortion produced by the human breast,'' J. Acoust. Soc. Am. **97**, 1958–1969 (1995).
[6] T. D. Mast, L. M. Hinkelman, M. J. Orr, V. W. Sparrow, and R. C. Waag, ''Simulation of ultrasonic pulse propagation through the abdominal wall,'' J. Acoust. Soc. Am. **102**, 1177–1190 (1997). [Erratum: **104**, 1124–1125 (1998).]
[7] J. Ylitalo, E. Alasaarela, and J. Koivukangas, ''Ultrasound holographic B-scan imaging,'' IEEE Trans. Ultrason. Ferroelectr. Freq. Control **36**, 376–383 (1989).
[8] K. E. Thomenius, ''Evolution of ultrasound beamformers,'' Proc. IEEE Ultrason. Symp. **2**, 1615–1622 (1996).
[9] L. M. Hinkelman, T. D. Mast, L. A. Metlay, and R. C. Waag, ''The effect of abdominal wall morphology on ultrasonic pulse distortion. Part I: Measurements,'' J. Acoust. Soc. Am. **104**, 3635–3649 (1998).
[10] S. W. Smith, G. E. Trahey, and O. T. von Ramm, ''Phased array ultrasound imaging through planar tissue layers,'' Ultrasound Med. Biol. **12**(3), 229–243 (1986).
[11] G. Kossoff, D. A. Carpenter, D. E. Robinson, D. Ostry, and P. L. Ho, ''A sonographic technique to reduce beam distortion by curved interfaces,'' Ultrasound Med. Biol. **15**(4), 375–382 (1989).
[12] M. O'Donnell and S. W. Flax, ''Phase-aberration correction using signals from point reflectors and diffuse scatterers: Measurements,'' IEEE Trans. Ultrason. Ferroelectr. Freq. Control **35**(6), 768–774 (1988).
[13] L. Nock, G. E. Trahey, and S. W. Smith, ''Phase aberration correction in medical ultrasound using speckle brightness as a quality factor,'' J. Acoust. Soc. Am. **85**, 1819–1833 (1989).
[14] D. Rachlin, ''Direct estimation of aberrating delays in pulse-echo imaging systems,'' J. Acoust. Soc. Am. **88**, 191–198 (1990).
[15] M. Hirama, O. Ikeda, and T. Sato, ''Adaptive ultrasonic array imaging through an inhomogeneous layer,'' J. Acoust. Soc. Am. **71**, 100–109 (1982).
[16] D.-L. Liu and R. C. Waag, ''Correction of ultrasonic wavefront distortion using backpropagation and a reference waveform method for time-shift compensation,'' J. Acoust. Soc. Am. **96**, 649–660 (1994).
[17] C. Dorme and M. Fink, ''Ultrasonic beam steering through inhomogeneous layers with a time reversal mirror,'' IEEE Trans. Ultrason. Ferroelectr. Freq. Control **43**(1), 167–175 (1996).
[18] T. D. Mast, ''Wideband quantitative ultrasonic imaging by time-domain diffraction tomography,'' J. Acoust. Soc. Am. **106**, 3061–3071 (1999).
[19] T. D. Mast, F. Lin, and R. C. Waag, ''Time-domain ultrasound diffraction tomography,'' *1999 IEEE Ultrasonics Symposium Proceedings*, Vol. 2, pp. 1617–1620.
[20] M. Slaney, A. C. Kak, and L. E. Larsen, ''Limitations of imaging with first-order diffraction tomography,'' IEEE Trans. Microwave Theory Tech. **32**, 860–874 (1984).
[21] F. Lin, A. I. Nachman, and R. C. Waag, ''Quantitative imaging using a time-domain eigenfunction method,'' J. Acoust. Soc. Am. **108**, 899–912 (2000).
[22] P. M. Morse and H. Feshbach, *Methods of Theoretical Physics* (McGraw-Hill, New York, 1953), Vol. I, Chap. 7.
[23] A. D. Pierce, *Acoustics: An Introduction to its Physical Principles and Applications*, 2nd ed. (Acoustical Society of America, Woodbury, NY, 1989), Chap. 9.
[24] G. Beylkin, ''The fundamental identity for iterated spherical means and the inversion formula for diffraction tomography and inverse scattering,'' J. Math. Phys. **24**, 1399–1400 (1983).
[25] C. Gasquet and P. Witomski, *Fourier Analysis and Applications: Filtering, Numerical Computation, Wavelets* (Springer-Verlag, New York, 1999).
[26] K. Kim and E. Wolf, ''Non-radiating monochromatic sources and their fields,'' Opt. Commun. **59**, 1–6 (1986).
[27] N. Bleistein and J. K. Cohen, ''Nonuniqueness in the inverse source problem in acoustics and electromagnetics,'' J. Math. Phys. **18**, 194–201 (1977).
[28] T. Melamed, Y. Ehrlich, and E. Heymann, ''Short-pulse inversion of inhomogeneous media: a time-domain diffraction tomography,'' Inverse Probl. **12**, 977–993 (1996).
[29] T. D. Mast, A. I. Nachman, and R. C. Waag, ''Focusing and imaging using eigenfunctions of the scattering operator,'' J. Acoust. Soc. Am. **102**, 715–725 (1997).
[30] V. A. Burov and O. D. Rumyantseva, ''Linearized inverse problem of scattering in monochromatic and pulse modes,'' Acoust. Phys. **40**, 34–42 (1996).
[31] T. T. Jansson, T. D. Mast, and R. C. Waag, ''Measurements of differential scattering cross section using a ring transducer,'' J. Acoust. Soc. Am. **103**, 3169–3179 (1998).
[32] P. M. Morse and K. U. Ingard, *Theoretical Acoustics* (McGraw-Hill, New York, 1968), Chap. 8.
[33] T. D. Mast, L. P. Souriau, D.-L. Liu, M. Tabei, A. I. Nachman, and R. C. Waag, ''A *k*-space method for large-scale models of wave propagation in

tissue,'' IEEE Trans. Ultrason. Ferroelectr. Freq. Control **48**, 341–354 (2001).
[34] T. D. Mast, ''Empirical relationships between acoustic parameters in human soft tissues,'' Acoust. Res. Lett. Online **1**, 37–42 (2000).
[35] J. L. Aroyan, ''Three-dimensional modeling of hearing in *Delphinus delphis*,'' J. Acoust. Soc. Am. **110**, 3305–3318 (2001).
[36] S. Wang, ''Finite-difference time-domain approach to underwater acoustic scattering problems,'' J. Acoust. Soc. Am. **99**, 1924–1931 (1996).
[37] M. Frigo and S. G. Johnson, ''FFTW: An adaptive software architecture for the FFT,'' *Proceedings of the ICASSP*, Vol. 3, pp. 1381–1384 (1998).
[38] W. H. Press, S. A. Teukolsky, W. T. Vetterling, and B. P. Flannery, *Numerical Recipes in Fortran* (Cambridge U.P., New York, 1986), Chap. 3.3.
[39] D. F. Rogers, *Procedural Elements for Computer Graphics* (McGraw–Hill, Boston, 1998), Chap. 2.
[40] A. E. Yagle and B. C. Levy, ''Layer-stripping solutions of multidimensional inverse scattering problems,'' J. Math. Phys. **27**, 1701–1710 (1986).
[41] Y. Chen, ''Inverse scattering via skin effect,'' Inverse Probl. **13**, 647–667 (1997).
[42] R. Snieder, ''A perturbative analysis of non-linear inversion,'' Geophys. J. Int. **101**, 545–556 (1990).
[43] J. A. Jensen and S. Leeman, ''Nonparametric estimation of ultrasound pulses,'' IEEE Trans. Biomed. Eng. **41**, 929–936 (1994).
[44] P. Lasaygues and J.-P. Lefebvre, ''Improvement of resolution in ultrasonic reflection tomography,'' The e-Journal of Nondestructive Testing **3**(8) (1998) [http://www.ndt.net/].
[45] O. Husby, T. Lie, T. Lango, J. Hokland, and H. Rue, ''Bayesian 2-D deconvolution: a model for diffuse ultrasound scattering,'' IEEE Trans. Ultrason. Ferroelectr. Freq. Control **48**, 121–130 (2001).